6ICEGE 6th International Conference on Earthquake Geotechnical Engineering
1-4 November 2015
Christchurch, New Zealand

Calibrating the Liquefaction Severity Number (LSN) for Varying Misprediction Economies: A Case Study in Christchurch, New Zealand

B. W. Maurer[1], R. A. Green[2], M. Cubrinovski[3] and B. A. Bradley[4]

ABSTRACT

Decision thresholds are central to the use of liquefaction hazard frameworks such as the liquefaction severity number (LSN). However, it is often unappreciated that proposed thresholds are inherently linked to: (1) the procedure used to compute FS_{liq} within the hazard framework; (2) the assessed dataset; and (3) as demonstrated herein, the approach used to select thresholds, and the assumed misprediction economies implicit to such selections. This study proposes a standardized approach by which the economies (i.e., consequences) of misprediction are used to make logical decisions with respect to hazard assessment. Optimum LSN decision thresholds are proposed for varying misprediction economies via an analysis of 7,000 liquefaction case studies from the Canterbury earthquakes. These thresholds strongly depend on underlying economic assumptions, with LSN = 15.4 being optimal when false positives and false negatives have similar costs. Assumed misprediction economies, implicit to all threshold hazard values proposed in the literature, could thus have significant implications for forward assessments of liquefaction hazard.

Introduction

The severity of soil liquefaction manifested at the ground surface (i.e., extensity/intensity of liquefaction ejecta and ground settlement) serves as a practical proxy for liquefaction damage potential, particularly for pavement systems, buried lifelines, structures on shallow foundations, and other near-surface infrastructure. The greater the severity of surficial manifestation, the greater the likelihood of damage to infrastructure. By way of this simplifying proxy, hazard frameworks have been proposed to link the factor of safety against liquefaction triggering at depth (FS_{liq}) to damage potential. Iwasaki et al. (1978) proposed the first such framework: the liquefaction potential index (LPI), which has been used to assess liquefaction hazards worldwide.

Though widely adopted, evaluations of LPI following recent liquefaction events, such as the 2010-2011 Canterbury Earthquake Sequence (CES), show that it performs inconsistently (e.g., Maurer et al., 2014). This inconsistency inspired the development of new hazard frameworks, to include an Ishihara (1985) inspired variation of LPI, termed LPI_{ISH} (Maurer et al., 2015a), and the liquefaction severity number (LSN) (van Ballegooy et al., 2014a), a variation of 1-dimensional post-liquefaction reconsolidation settlement (e.g., Zhang et al., 2002). Central to all of these hazard frameworks are proposed decision thresholds corresponding to different levels of expected hazard. For example, Iwasaki (1986) proposed that liquefaction hazard is "low" at sites where $LPI \leq 5$, "high" where $5 < LPI \leq 15$, and "very high" where $LPI > 15$. Similarly, Tonkin

[1]Graduate Student, Dept. of Civil Eng., Virginia Tech, Blacksburg, Virginia, USA, bwmaurer@vt.edu
[2]Prof., Dept. of Civil Eng., Virginia Tech, Blacksburg, Virginia, USA, rugreen@vt.edu
[3]Prof., Dept. of Civil Eng., University of Canterbury, Christchurch, NZ, misko.cubrinovski@canterbury.ac.nz
[4]Assoc. Prof., Dept. of Civil Eng., University of Canterbury, Christchurch, NZ, brendon.bradley@canterbury.ac.nz

and Taylor (2013) proposed that little to no manifestation of liquefaction is expected at sites where LSN < 20; moderate to severe manifestation of liquefaction is expected where 20 < LSN < 40; and major manifestation of liquefaction is expected where LSN > 40. Thus, an LPI of 5 and an LSN of 20 correspond to similar levels of expected hazard. Importantly, it is often unappreciated that these proposed thresholds are inherently linked to: (1) the procedure used to compute FS_{liq} within the hazard framework; (2) the assessed dataset; and (3) the technique used to select thresholds, and the assumed misprediction consequences implicit to any such selection.

First, several liquefaction evaluation procedures are commonly used in today's practice to compute FS_{liq}, an input to the aforementioned hazard frameworks (e.g., Boulanger and Idriss (2014) vs. Idriss and Boulanger (2008) vs. Moss et al. (2006) vs. Robertson and Wride (1998) and so forth). It has been shown that these procedures can yield different FS_{liq} values for the same soil profile and earthquake scenario (e.g., Green et al., 2014), and thus different hazard values (Lee et al., 2003; Maurer et al., 2015b). For example, using data from the CES, Maurer et al. (2015b) compared the efficacy of the Robertson and Wride (1998), Moss et al. (2006), and Idriss and Boulanger (2008) procedures, operating within the LPI framework, for predicting the severity of liquefaction manifestation. The relationship between manifestation severity and computed LPI values was found to be specific to the procedure used to compute FS_{liq} (e.g., the hazard corresponding to LPI = 5 varied amongst the procedures). Thus, threshold hazard values proposed using one procedure to compute FS_{liq} may be less than optimum when using another.

Second, proposed threshold values are inherently linked to the properties of the assessed dataset, to include the stratigraphy and soil characteristics of site-profiles, as well as the amplitude and duration of ground shaking (Juang et al., 2008; Kang et al., 2014; Maurer et al., 2015b,c). For example, in analyzing data from the CES, Maurer et al. (2015c) compared threshold LPI values for sites inferred to have predominantly clean sand or silty sand with sites inferred to have predominantly silty and clayey soil mixtures. Sites in the latter group had a significantly higher optimum threshold LPI for predicting liquefaction manifestation (LPI = 13.0) than those in the former group (LPI = 4.9), irrespective of which procedure was used to compute FS_{liq}. Similar discrepancies can be found among other LPI studies (Maurer et al., 2015c). Thus, threshold hazard values proposed using one dataset may be less than optimum when applied to another.

Third, authors have used different methods and justifications to select optimum decision thresholds. For example, Iwasaki et al. (1982) found that of 55 sites evaluated, 80% of sites with liquefaction manifestation had LPI > 5, and 70% of sites without manifestation had LPI < 5; this led Iwasaki et al. (1982) to propose LPI = 5 as an optimum threshold. While some studies have used similar methodologies, others have used unstated justifications. Further, implicit to all proposed thresholds are assumed economies of misprediction. For example, Iwasaki et al. (1978) implicitly treated the costs of false positives (i.e., liquefaction manifestation is predicted but is not observed) and false negatives (i.e., liquefaction manifestation is observed when it is not predicted) to be similar. Had Iwasaki et al. (1982) instead assumed that false negatives were significantly more costly (a reasonable assumption for many engineering projects), the proposed LPI threshold would presumably have been less than LPI = 5. Authors assuming different misprediction economies will invariably propose different decision thresholds. Thus, the lack of a standardized approach to selecting threshold values complicates comparisons amongst studies.

Due to the combined effects of the above, proposed thresholds vary significantly for the same

hazard framework and equivalent hazard levels. For example, Iwasaki et al. (1982), Toprak and Holzer (2003), Lee et al. (2003), Papathanassiou (2008), Kang et al. (2014), Papathanassiou et al. (2015), and Maurer et al. (2015b), each using data from different earthquakes, proposed LPI thresholds for predicting liquefaction manifestation of 5, 5, 13, 14, 14, ~13.5, and 5, respectively. While recent studies have investigated factors responsible for such discrepancies, the significance of assumed misprediction economies has not been assessed. Clearly, the conservatism desired in any hazard assessment must consider the consequences of misprediction, which vary amongst engineering projects. It follows then that decision thresholds should be applied on a project-specific basis, since the threshold hazard value that is "optimum" for one project, or one category of infrastructure, may be inappropriate for others.

Accordingly, this study proposes a simple and standardized approach by which the economies (i.e., consequences) of misprediction can be used to make rational decisions with respect to hazard assessment. The proposed approach is an extension of the receiver-operating-characteristic (ROC) methodology used by Maurer et al. (2015b,c) to standardize the selection of threshold hazard values. Using this approach, optimum LSN decision thresholds are proposed for varying misprediction economies via an analysis of 7,000 liquefaction case studies from the 2010-2011 Canterbury earthquakes. This analysis is performed using the Idriss and Boulanger (2008) liquefaction evaluation procedure to compute FS_{liq}. While the proposed approach is herein applied to LSN, now widely used in New Zealand, it is applicable to any hazard framework. In the following, the proposed ROC methodology is first developed, followed by a summary of the CES dataset and proposal of LSN decision thresholds.

Receiver Operating Characteristic (ROC) Framework

ROC analyses are a simple but powerful method for evaluating the relative efficacy of competing diagnostic tests, independent of the thresholds used, and for selecting an optimal threshold for a given diagnostic test. In using LSN to predict liquefaction manifestation, the distributions of "positives" (i.e., liquefaction manifestation is observed) and "negatives" (i.e., no liquefaction manifestation is observed) overlap when the frequencies of the distributions are expressed in terms of computed LSN values. Ideally, LSN decision thresholds should then be selected considering both the rate and consequence of mispredictions (i.e., false positives and false negatives). Setting the decision threshold too low or too high will result in a greater number of mispredictions; the degree to which these mispredictions are acceptable is a function of their consequences, or costs. The cost of a false positive might be the superfluous spending on engineering design and construction (e.g., ground improvement costs), while the cost of a false negative might be the costs of liquefaction-induced damage (e.g., lost productivity, property damage, and reconstruction costs, among others).

ROC curves plot the rates of true positives (R_{TP}) versus false positives (R_{FP}) for varying threshold values. Figures 1a and 1b illustrate the relationship among the positive and negative distributions, the threshold value, and the ROC curve. Figure 1b also illustrates how a ROC curve is used to assess the efficiency of a diagnostic test and select an optimum threshold. In ROC space, random guessing is indicated by a 1:1 line through the origin (i.e., equivalent correct and incorrect predictions), while a perfect model plots as a point at (0,1), indicating the existence of a threshold value which perfectly segregates the dataset (i.e., all cases with manifestation have LSN above the threshold; all cases without manifestation have LSN below the threshold).

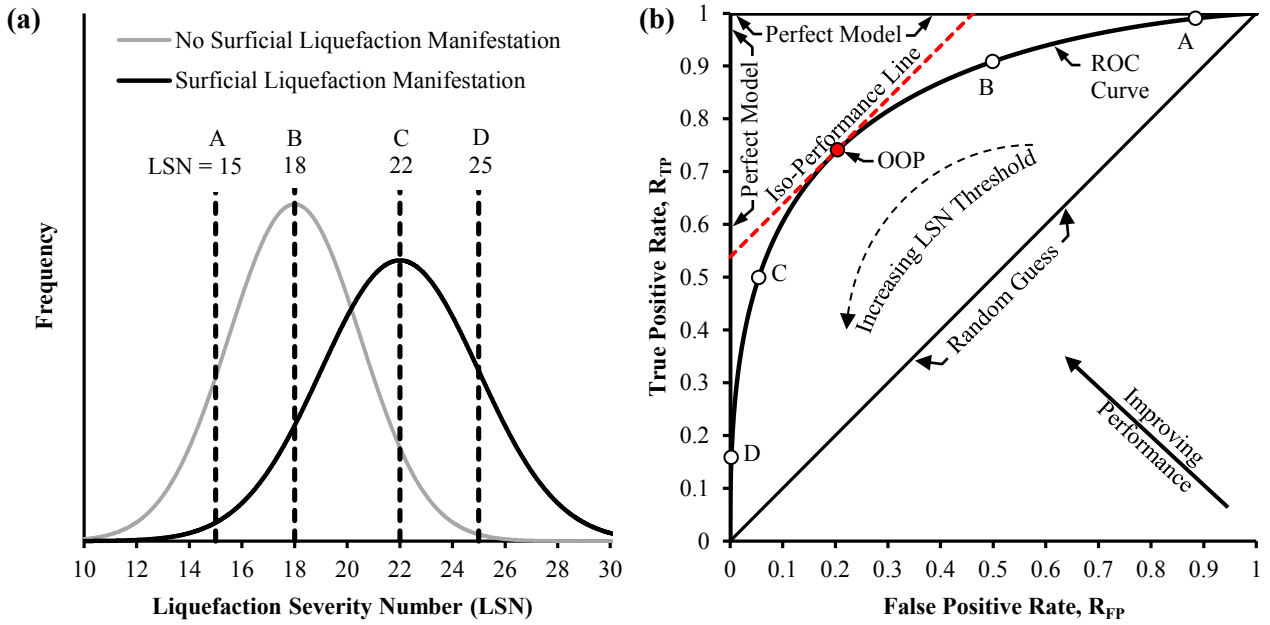

Figure 1: ROC analyses: (a) frequency distributions of liquefaction manifestation and no liquefaction manifestation as a function of LSN; (b) corresponding ROC curve, and illustration of how a ROC curve is used to assess the efficiency of a diagnostic test.

The optimum operating point (OOP) indicates the LSN decision threshold for which the misprediction cost is minimized. The optimum decision threshold, or optimum operating point (OOP), is defined herein as the threshold LSN value which minimizes the cost of misprediction, where cost is computed as:

$$\text{Cost} = C_{FP} \text{ x } R_{FP} + C_{FN} \text{ x } R_{FN} \quad (1)$$

where C_{FP} and R_{FP} are the cost and rate of false positive predictions, respectively, and C_{FN} and R_{FN} are the cost and rate of false negative predictions, respectively. Normalizing with respect to C_{FN}, Equation (1) may alternatively be expressed as:

$$\text{Cost'} = \text{Cost}/C_{FN} = R_{FP} \text{ x CR} + R_{FN} \quad (2)$$

where CR is the *cost ratio* defined by $CR = C_{FP} / C_{FN}$. In Equations (1) and (2), the rates of false negatives (R_{FN}) and false positives (R_{FP}) are respectively defined by:

$$R_{FN} = Q_{FN} / (Q_{FN} + Q_{TP}) \quad (3a)$$

$$R_{FP} = Q_{FP} / (Q_{FP} + Q_{TN}) \quad (3b)$$

where Q_{TP}, Q_{FP}, Q_{TN}, and Q_{FN} are respectively the quantities of true positives, false positives, true negatives, and false negatives. Thus, the denominators of Equations (3a) and (3b) equal the total number of sites with and without observed surficial liquefaction manifestations, respectively. Accordingly, the rate of true positives (R_{TP}) is equal to 1-R_{FN} and the rate of true negatives (R_{TN}) is equal to 1-R_{FP}. Since cost-contours represent points of equivalent performance (i.e., equal Cost') in ROC space, it follows from Equations (1-3) that two points in ROC space,

(R_{FP1}, R_{TP1}) and (R_{FP2}, R_{TP2}) have equivalent performance if:

$$\frac{R_{TP1} - R_{TP2}}{R_{FP1} - R_{FP2}} = \frac{C_{FP}}{C_{FN}} = CR = m \quad (4)$$

Equation (4) defines the slope, *m*, of an iso-performance line, such that all points defining the line have the same expected Cost' (Provost and Fawcett, 2001). Thus, each unique CR corresponds to a different iso-performance line in ROC space. One such iso-performance line is shown in Fig. 1b. With 1:1 slope, this line corresponds to the case where false positives and false negatives have equivalent Cost' (i.e., CR = 1). Iso-performance points tangential to the ROC curve correspond to optimum threshold values for the classifier (i.e., OOPs). Thus, the OOP identified in Figure 1b accounts for both the rates and consequences of misprediction. Repeating for different values of CR, varying misprediction economies can be used to select optimum LSN decision thresholds.

Data and Methodology

CPT soundings

This study utilizes 3,500 CPT soundings performed at sites where the severity of liquefaction manifestation was well-documented following both the Darfield and Christchurch earthquakes, resulting in 7,000 liquefaction case studies. In the process of compiling these case studies, CPT soundings were first rejected from the study: (1) if performed at sites where the predominant manifestation of liquefaction was lateral spreading; (2) if the depth of "pre-drill" significantly exceeded the estimated depth of the ground water table, a condition arising at sites where buried utilities needed to be safely bypassed before testing could begin; and (3) if believed to have prematurely terminated on shallow gravels, as inferred from an Anselin (1995) Local Morans *I* analysis. For further discussion of CPTs and this geostatistical analysis, see Maurer et al. (2014).

Liquefaction severity

Observations of liquefaction and the severity of manifestation were made by the authors for each of the CPT sounding locations following both the Darfield and Christchurch earthquakes. CPT sites were assigned one of six damage classifications, as described in Green et al. (2014). Of the 7,000 cases compiled, 49% are cases of "no manifestation," and 51% are cases where manifestations were observed and classified in accordance with Green et al. (2014). It should be noted that free-field surface manifestation is a simplifying proxy for damage potential. While it has been shown that factors controlling damage are structure-, soil-, and earthquake-specific (e.g., Dashti and Bray, 2014), no practical method yet exists for incorporating all these factors.

Estimation of peak ground acceleration (PGA)

To evaluate FS_{liq} for use in computing LSN values, the Peak Ground Accelerations (PGAs) at the ground surface were computed using the procedure discussed in detail by Bradley (2013a) and used by Green et al. (2014) and Maurer et al. (2014, 2015b,c). The Bradley (2013a) procedure combines unconditional PGA distributions estimated by the Bradley (2013b) ground motion prediction equation, recorded PGAs from strong motion stations, and the spatial correlation of intra-event residuals to compute the conditional PGA distribution at sites of interest.

Estimation of ground-water table (GWT) depth

Given the sensitivity of liquefaction hazard to GWT depth (e.g., Chung and Rogers, 2011; Maurer et al., 2014), accurate measurement of the GWT is critical. For this study, GWT depths were sourced from the robust, event-specific regional ground water models of van Ballegooy et al. (2014b). These models, which reflect seasonal and localized fluctuations across the region, were derived in part using monitoring data from a network of ~1000 piezometers and provide a best-estimate of GWT depths immediately prior to the Darfield and Christchurch earthquakes.

Liquefaction Evaluation and LSN

FS_{liq} was computed using the deterministic procedure proposed by Idriss and Boulanger (2008)[I&B08], where the soil behavior type index, I_c, was used to identify non-liquefiable strata; soils with $I_c > 2.4$ were assumed non-liquefiable, per Maurer et al. (2015c). For I&B08, fines content (FC) is required to compute normalized tip resistances; as such, FC values were estimated using the I_c-FC correlation proposed by Boulanger and Idriss (2014). LSN was computed for each of the 7,000 case studies per Equation (5) (van Ballegooy et al., 2014a), where ε_v is the estimated post-liquefaction volumetric strain (%), as computed by the Zhang et al. (2002) method, and z is depth (m) below the ground surface.

$$\mathrm{LSN} = 10 \int_0^{20\ \mathrm{m}} \epsilon_v / z \ \mathrm{dz} \tag{5}$$

Results and Discussion

In Figure 2a, ROC curves are plotted to evaluate LSN's performance in predicting liquefaction manifestations likely to damage infrastructure. In our classification scheme (Green et al., 2014), marginal manifestations are characterized by a trace amount of water or ejecta and are thus likely to be non-damaging. Conversely, moderate to severe manifestations are more likely to coincide with damage to infrastructure. Failure to accurately assess such hazards could result in either: (1) superfluous spending on engineering design and construction, in the case of a false-positive prediction; or (2) severe damage to infrastructure, in the case of a false-negative prediction. Highlighted in Figure 2a is the optimal LSN threshold for the case of CR = 1, which is reasonably consistent with that proposed by Tonkin and Taylor (2013) (i.e., LSN = 20). Repeating for a range of CR values, optimal LSN thresholds are plotted in Figure 2b as a function of CR, such that project-specific economies can be used to select optimal decision thresholds; in this way, selection of an LSN threshold is analogous to selecting an appropriate level of conservatism. To demonstrate, consider a structure with a 100 year design life. From CPT soundings at the site, LSN is computed by I&B08 to be 8.0 for a 25 year return-period earthquake, which, assuming a Poisson distribution, has a 98% probability of occurring in 100 years. If the structure is modest and CR is estimated to be 0.55 (e.g., assuming: (1) moderate-to-severe liquefaction causes $60,000 in damages; and (2) ground improvement and/or robust construction to mitigate the hazard costs $33,000), the optimal decision threshold is LSN = 11.3 (Figure 2b). Since the computed LSN at the site is less than the optimum threshold, the scenario should be treated as "non-hazardous." Conversely, if the structure is a critical facility with CR = 0.15, the optimal threshold is LSN = 3.1. In this case, paying the cost of a false-negative up-front is advised. While this simple example does not justly represent the complexity and probabilistic

nature of life-cycle cost analyses (e.g., consideration of earthquake motions for a range of return periods), it demonstrates that some consideration should be given to the relative consequences of misprediction when selecting a decision threshold.

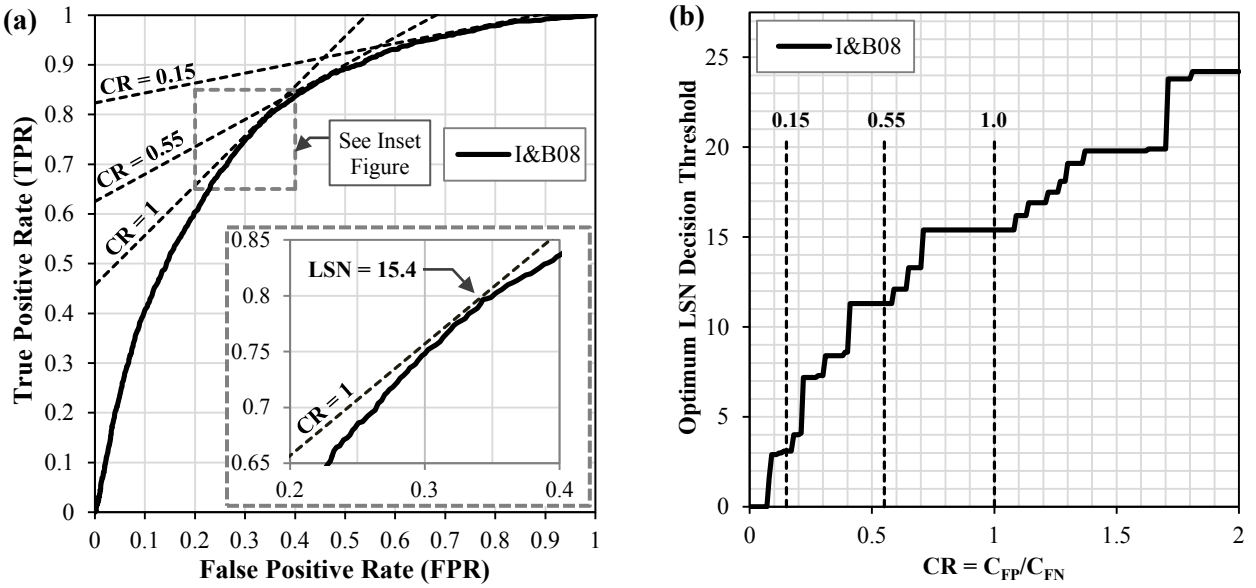

Figure 2: (a) ROC analysis of LSN performance in predicting liquefaction likely to cause damage, with optimal threshold LSN highlighted for CR = 1; (b) optimal LSN threshold vs. CR.

Conclusions

This study proposed a framework by which the consequences of misprediction can be used to make logical decisions with respect to liquefaction hazard assessment. Optimal LSN decision thresholds were proposed for varying misprediction costs using 7,000 case studies. Moreover, it was shown that while often unrealized, assumed costs are implicit to all proposed decision thresholds in the literature; as shown in Figure 2b, this assumption can significantly influence the optimal threshold. The findings presented in this study are based on a dataset from the CES; their applicability to other datasets, or to methodologies different from that used herein, is unknown.

Acknowledgments

This study is based on work supported by the US National Science Foundation (NSF) grants CMMI 1030564, CMMI 1407428, and CMMI 1435494, and US Army Engineer research and Development Center (ERDC) grant W912HZ-13-C-0035. The authors also acknowledge the Canterbury Geotechnical Database and its sponsor EQC for providing data used in this study. However, any opinions, findings, and conclusions or recommendations expressed in this paper are those of the authors and do not necessarily reflect the views of NSF, ERDC, or EQC.

References

Anselin L. Local Indicators of Spatial Association—LISA. *Geographical Analysis* 1995; **27** (2): 93–115.

Boulanger RW, Idriss IM. CPT and SPT based liquefaction triggering procedures. *Report No. UCD/CGM-14/01*, Center for Geotech. Modeling, Dept. of Civil and Environ. Eng., University of California, Davis, CA; 2014.

Bradley BA. Site-specific and spatially-distributed ground motion intensity estimation in the 2010-2011 Christchurch earthquakes. *Soil Dynamics and Earthquake Engineering* 2013a; **48**: 35-47.

Bradley BA. A New Zealand-specific pseudo-spectral acceleration ground-motion prediction equation for active shallow crustal earthquakes based on foreign models. *BSSA* 2013b; **103**(3): 1801-1822.

Chung J, Rogers J. Simplified method for spatial evaluation of liquefaction potential in the St. Louis Area. *J Geotech Geoenviron Eng* 2011; **137**(5): 505-515.

Dashti S and Bray JD. Numerical simulation of building response on liquefiable sand. *J Geotech Geoenviron Eng* 2013; **139**(8): 1235-1249.

Green, RA, Cubrinovski, M, Cox, B, Wood, C, Wotherspoon, L, Bradley, B, Maurer, B. Select Liquefaction Case Histories from the 2010-2011 Canterbury Earthquake Sequence. *Earthquake Spectra* 2014; **30**(1): 131-153.

Idriss IM, Boulanger RW. Soil liquefaction during earthquakes. *Monograph MNO-12* 2008; Earthquake Engineering Research Institute, Oakland, CA, 261 pp.

Ishihara, K. Stability of natural deposits during earthquakes. In: *Proceedings of the 11th International Conference on Soil Mechanics and Foundation Engineering* 1985; San Francisco, CA, USA, 1, 321-376.

Iwasaki T. Soil liquefaction studies in Japan: state-of-the-art. *Soil Dynamics and Earthquake Eng* 1986; **5**(1): 2-68.

Iwasaki, T, Tatsuoka, F, Tokida, K, and Yasuda, S. A practical method for assessing soil liquefaction potential based on case studies at various sites in Japan. *Proc. 2nd Int. Conf. on Microzonation*, San Francisco, USA; 1978.

Iwasaki T, Tokida K, Tatsuoka, F, Watanabe, S, Yasuda S, and Sato, H. A practical method for assessing soil liquefaction potential based on case studies at various sites in Japan. *Proc. 3rd Int. Conf. on Microzonation*, Seattle, USA; 1982.

Juang, CH, Liu, CN, Chen, CH, Hwang, JH, and Lu, CC. Calibration of liquefaction potential index: a re-visit focusing on a new CPTU model. *Engineering Geology* 2008 **102**: 19–30.

Kang GC, Chung JW, Rogers JD. Re-calibrating the thresholds for the classification of liquefaction potential index based on the 2004 Niigata-ken Chuetsu earthquake. *Engineering Geology* 2014; **169**: 30-40.

Lee DH, Ku CS, Yuan H. A study of liquefaction risk potential at Yuanlin, Taiwan. *Eng Geology* 2003; **71**:97-117.

Maurer BW, Green RA, Cubrinovski M, Bradley B. Evaluation of the liquefaction potential index for assessing liquefaction hazard in Christchurch, New Zealand. *J Geotech Geoenviron Eng* 2014; **140**(7), 04014032.

Maurer BW, Green RA, Cubrinovski M, Bradley B. Moving towards an improved index for assessing liquefaction hazard: lessons from historical data. *Soils and Foundations* 2015a; *In Press,* doi:10.1016/j.sandf.2015.06.010.

Maurer BW, Green RA, Cubrinovski M, Bradley B. Assessment of CPT-based methods for liquefaction evaluation in a liquefaction potential index (LPI) framework. *Geotechnique* 2015b; **65**(5): 328-336.

Maurer BW, Green RA, Cubrinovski M, Bradley B. Fines-content effects on liquefaction hazard evaluation for infrastructure during the 2010-2011 Canterbury, New Zealand earthquake sequence. *Soil Dynamics and Earthquake Engineering* 2015c; **76***:* 58-68.

Moss RES, Seed RB, Kayen RE, Stewart JP, Der Kiureghian A, Cetin KO. CPT-based probabilistic and deterministic assessment of in situ seismic soil liquefaction potential. *J Geotech Geoenviron Eng* 2006; **132** (8): 1032-1051.

Papathanassiou G. LPI-Based Approach for Calibrating the Severity of Liquefaction-Induced Failures and for Assessing the Probability of Liquefaction Surface Evidence. *Engineering Geology 2008*; **96**: 94-104.

Papathanassiou G, Mantovani A, Tarabisu G, Rapti D, and Caputo R. Assessment of liquefaction potential for two liquefaction prone areas considering the May 20, 2012 Emilia (Italy) earthquake. *Eng Geology* 2015; **189**: 1-16.

Provost F, Fawcett T. Robust classification for imprecise environments. *Machine Learning* 2001; **42** (3): 203–231.

Robertson PK, Wride CE. Evaluating cyclic liquefaction potential using cone penetration test. *Canadian Geotechnical Journal* 1998; **35** (3): 442-459.

Tonkin & Taylor Ltd. Liquefaction vulnerability study. *T&T Ref: 52020.0200/v.1.0*, Christchurch, NZ, 2013.

Toprak, S, Holzer, T. Liquefaction potential index: field assessment. *J Geotech Geoenviron Eng* 2003; **129**(4): 315-322.

van Ballegooy, S, Malan, P, Lacrosse, V, Jacka, ME, Cubrinovski, M, Bray, JD, O'Rourke, TD, Crawford, SA, and Cowan, H. Assessment of liquefaction-induced land damage for residential Christchurch. *Earthquake Spectra*, 2014a; **30**(1): 31-55.

van Ballegooy S, Cox SC, Thurlow C, Rutter HK, Reynolds T, Harrington G, Fraser J, and Smith T. Median water table elevation in Christchurch and surrounding area after the 4 September 2010 Darfield earthquake: Version 2. *GNS Science Report 2014/18*, 2014b.

Zhang G, Robertson PK, Brachman R. Estimating Liquefaction Induced Ground Settlements from CPT. *Canadian Geotechnical Journal* 2002; **39**: 1168-1180.